Tribology International 94 (2016) 288–305

Contents lists available at ScienceDirect

Tribology International

journal homepage: www.elsevier.com/locate/triboint

Dynamic characteristics of compliant journal bearings considering thermal effects

Evgeny Kuznetsov [a,b], Sergei Glavatskih [a,c,*]

[a] Machine Design, KTH Royal Institute of Technology, Stockholm, Sweden
[b] COMSOL LLC, Moscow, Russia
[c] Mechanical Construction and Production, Ghent University, Ghent, Belgium

ARTICLE INFO

Article history:
Received 4 April 2015
Received in revised form
7 July 2015
Accepted 9 August 2015
Available online 17 August 2015

Keywords:
Stiffness
Damping
Compliance
Thermal effects

ABSTRACT

A numerical THD model that takes into account mechanical and thermal deformations of a compliant lining is used to investigate the influence of compliance on dynamic characteristics of a two axial groove bearing. A detailed study on the contribution of mechanical and thermal deformation components of the compliant lining to the non-dimensional bearing stiffness and damping is carried out. Thermal deformation is found to increase horizontal stiffness K_{yy} and cross-coupled stiffness K_{xy} and slightly reduce journal critical mass. Mechanical deformation of the compliant lining is found to decrease damping, reduce vertical and cross-coupled K_{xy} stiffness. Radial clearance is found to increase stiffness, except its horizontal component, and decrease horizontal damping. Compliant lining is found to improve bearing stability.

1. Introduction

Hydrodynamic journal bearings are routinely used in a wide range of industrial machinery. Such bearings are relatively simple to manufacture and easy to install. They provide higher damping and take less space if compared to rolling element bearings. A general trend in machine elements is to increase power density by making components smaller and to reduce power consumption. One way to achieve lower power losses in a journal bearing is to use oils with better viscosity-temperature characteristics and higher oxidation stability as shown in [1]. Another promising approach is to substitute babbitt by a low friction compliant material. It was shown that a polytetrafluoroethylene (PTFE) facing on tilting pads improved thrust bearing full film operation [2–4]. PTFE is also capable of providing lower friction during short periods of boundary and mixed lubrication that occur during start-ups and shutdowns [5].

As explained in [6] a PTFE lining in a journal bearing improves steady state performance characteristics in comparison with a babbitted bearing. A compliant lining enhances bearing load carrying capacity, decreases maximum pressure and increases minimum oil film thickness while power losses and maximum film temperature remain similar or slightly increase [6]. A positive effect of bearing compliance is also known in foil gas bearings [7,8].

Since a PTFE lining is more elastic than babbitt, bearing dynamic characteristics will be affected. Stability of the plain journal bearings with compliant linings has been studied by several authors. Since nonlinear analysis is not the scope of the present paper, we only consider papers relevant to the linearized approach. Most of the published works refer to the work of Lund and Thomsen [9] when new numerical models are validated. In 1978 Lund and Thomsen [9] published an algorithm to evaluate linearized stiffness and damping coefficients for conventional plain journal bearings in the isoviscous conditions. Zhang et al. modified Lund's original approach to analyse a compliant lining bearing in the isothermal case in terms of journal critical mass and whirl ratio [10]. The dynamic deformation of the lining was shown to be important in the linear stability analysis. The same trend was also shown by [11,12]. Rao et al. [13] published an analytical approach for a quick estimation of linearized stiffness and damping for an iso-viscous problem. Results were verified by a comparison with Lund's data [9].

* Corresponding author at: Machine Design, KTH Royal Institute of Technology, Stockholm, Sweden.
E-mail address: segla@kth.se (S. Glavatskih).

http://dx.doi.org/10.1016/j.triboint.2015.08.018
0301-679X/

List of symbols

$B_{xx}, B_{yx}, B_{xy}, B_{yy}$	Damping coefficients (Ns/m)
C	bearing radial clearance (m)
E	PTFE Young's modulus (Pa)
h	oil film thickness (m)
k_0	effective bearing stiffness (N/m)
$K_{xx}, K_{yx}, K_{xy}, K_{yy}$	stiffness coefficients (N/m)
M_{crit}	critical journal mass (kg)
p	oil film pressure (Pa)
r	journal radius (m)
s	compliant lining thickness (m)
t	time (s)
W	load carrying capacity (N)
y	cross-film coordinate (m)
z	axial coordinate (m)
δ	deformation of the compliant lining (m)
ε	eccentricity (m)
θ	circumferential coordinate (rad)
ϑ	instability whirl frequency (rad/s)
μ	oil viscosity (Pas)
ν	Poisson's ratio (-)
φ	attitude angle (rad)
Ω	journal speed (RPM)

Constants and non-dimensional parameters

B_r	$\frac{\mu_0 \cdot \omega^2 \cdot R^2}{K_h \cdot T_0}$
B_{xx}	$\overline{B}_{xx}\frac{W}{\omega C}$
e	ε/C
$\overline{h}$	h/C
K_{xx}	$\overline{K}_{xx}\frac{W}{C}$
$\overline{r}$	r/R
$\overline{t}$	$t\omega$
$\overline{y}$	y/h
$\overline{z}$	z/L
η	R/L
θ	x/R
$\overline{\mu}$	μ/μ_0
$\overline{v}$	$v/\omega h$
ω	$\pi\Omega/30$

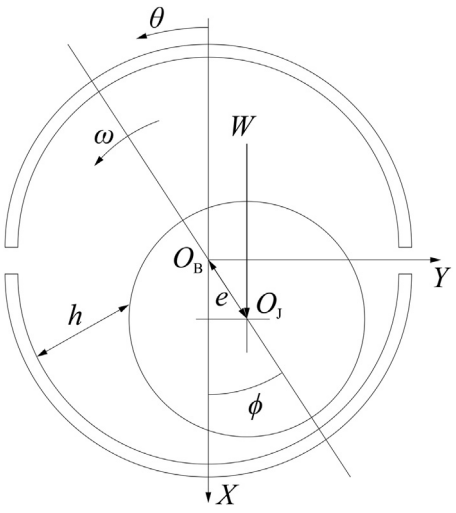

Fig. 1. Bearing geometry.

Recently, several authors published hydrodynamic and elastohydrodynamic studies of bearings with compliant linings, confirming the importance of the dynamic deformation in the stability analysis [14,15]. The compliant lining was shown to increase minimum film thickness, decrease stiffness, damping, load carrying capacity and attitude angle at a fixed relative eccentricity [14]. The cross-coupling damping coefficients were shown to be different if compliant lining is implemented [15]. This was also observed in the earlier works [10–12].

Durany et al. [16] used a thermohydrodynamic model to analyse dynamic behaviour of a plain journal bearing. Mechanical deformation of the bearing was not considered. Journal critical mass was shown to be increased if difference between shaft and bearing temperatures was positive and increased. At the same time, if shaft temperature was lower then that of the bearing, the journal critical mass was shown to be lower then that in the hydrodynamic model.

While journal bearing dynamic analysis has been extensively done for iso-viscous conditions with and without the effect of elasticity, a proper thermoelastohydrodynamic analysis seems to be missing. Moreover, the thermal effects were shown to have a visible influence on the linearized dynamic characteristics of the plain journal bearings [16].

The goal of this work is to analyse the effect of lining compliance on the stiffness, damping and stability of a plain cylindrical bearing using a thermoelastohydrodynamic bearing model. This work is a continuation of the work reported in [6].

2. Model description

The numerical model consists of two parts: a static analysis to obtain the journal equilibrium position and a dynamic analysis to evaluate stiffness and damping coefficients. Since the first part is well described in [17], we present only a short summary here. The

journal equilibrium position is found by solving a hydrodynamic problem with thermal effects and mechanical deformations taken into account. The Reynolds equation with a 3D viscosity variation, 3D energy and 3D heat transfer equations are solved. Zero boundary conditions are imposed at the bearing edges. Bearing geometry is shown in Fig. 1.

Mixing coefficients are used to evaluate oil temperature in the bearing supply grooves [17]. Plain strain hypothesis is used to evaluate mechanical deformation of the lining. Accuracy of this method is acceptable as shown in [18].

A linear dynamic analysis is usually performed by using a perturbation approach, proposed by Lund [9]. We modified this approach so that it can be used for compliant bearings [12].

At first, we introduce small time-dependent perturbations

$$h_P = \Delta x \cos\theta + \Delta y \sin\theta, \tag{1}$$

and rewrite pressure in the following way:

$$p = p_0 + p_x \Delta x + p_y \Delta y + p'_x \Delta\dot{x} + p'_y \Delta\dot{y}. \tag{2}$$

Next, we add perturbations and the deformation of the compliant lining to the initial film thickness h_0

$$h = h_0 + h_P + F_{def}(p), \tag{3}$$

By F_{def} we denote a function that describes deformation generated by hydrodynamic pressure:

$$F_{def}(p) = \frac{s \cdot p}{E} \frac{(1+\nu)(1-2\nu)}{1-\nu} \tag{4}$$

Then we consider the Reynolds equation with time component taken into account

$$\frac{\partial}{\partial\theta}\left(\overline{Gh}^3 \frac{\partial\overline{p}}{\partial\theta}\right) + \eta\frac{\partial}{\partial\overline{z}}\left(\overline{Gh}^3 \frac{\partial\overline{p}}{\partial\overline{z}}\right) = \frac{\partial\left(\overline{h} - \overline{h}^{\overline{I}}_{\overline{j}}\right)}{\partial\theta} + \frac{\partial\overline{h}}{\partial\overline{t}}, \tag{5}$$

Substituting (2) and (3) into (5) and retaining only the first order terms we obtain the following equations:

$$\frac{\partial}{\partial\theta}\left(\overline{G}\left(\overline{h}_0 + F_{def}(\overline{p}_0)\right)^3 \frac{\partial\overline{p}_0}{\partial\theta}\right) + \eta\frac{\partial}{\partial\overline{z}}\left(\overline{G}\left(\overline{h}_0 + F_{def}(\overline{p}_0)\right)^3 \frac{\partial\overline{p}_0}{\partial\overline{z}}\right) = \frac{\partial\left(\left(\overline{h}_0 + F_{def}(\overline{p}_0)\right)\left(1 - \frac{\overline{I}}{\overline{j}}\right)\right)}{\partial\theta}, \tag{6}$$

$$\begin{aligned}&\frac{\partial}{\partial\theta}\left(\overline{G}\left(\overline{h}_0 + F_{def}(\overline{p}_0)\right)^3 \frac{\partial\overline{p}_x}{\partial\theta}\right) + \eta\frac{\partial}{\partial\overline{z}}\left(\overline{G}\left(\overline{h}_0 + F_{def}(\overline{p}_0)\right)^3 \frac{\partial\overline{p}_x}{\partial\overline{z}}\right) = \frac{\partial\left(\left(\cos\theta + F_{def}(\overline{p}_x)\right)\left(1 - \frac{\overline{I}}{\overline{j}}\right)\right)}{\partial\theta}\\ &-3\frac{\partial}{\partial\theta}\left(\overline{G}\left(\cos\theta + F_{def}(\overline{p}_x)\right)\left(\overline{h}_0 + F_{def}(\overline{p}_0)\right)^2 \frac{\partial\overline{p}_0}{\partial\theta}\right) - 3\eta\frac{\partial}{\partial\overline{z}}\left(\overline{G}\left(\cos\theta + F_{def}(\overline{p}_x)\right)\left(\overline{h}_0 + F_{def}(\overline{p}_0)\right)^2 \frac{\partial\overline{p}_0}{\partial\overline{z}}\right),\end{aligned} \tag{7}$$

$$\begin{aligned}&\frac{\partial}{\partial\theta}\left(\overline{G}\left(\overline{h}_0 + F_{def}(\overline{p}_0)\right)^3 \frac{\partial\overline{p}_y}{\partial\theta}\right) + \eta\frac{\partial}{\partial\overline{z}}\left(\overline{G}\left(\overline{h}_0 + F_{def}(\overline{p}_0)\right)^3 \frac{\partial\overline{p}_y}{\partial\overline{z}}\right) = \frac{\partial\left(\left(\sin\theta + F_{def}\left(\overline{p}_y\right)\right)\left(1 - \frac{\overline{I}}{\overline{j}}\right)\right)}{\partial\theta}\\ &-3\frac{\partial}{\partial\theta}\left(\overline{G}\left(\sin\theta + F_{def}\left(\overline{p}_y\right)\right)\left(\overline{h}_0 + F_{def}(\overline{p}_0)\right)^2 \frac{\partial\overline{p}_0}{\partial\theta}\right) - 3\eta\frac{\partial}{\partial\overline{z}}\left(\overline{G}\left(\sin\theta + F_{def}\left(\overline{p}_y\right)\right)\left(\overline{h}_0 + F_{def}(\overline{p}_0)\right)^2 \frac{\partial\overline{p}_0}{\partial\overline{z}}\right),\end{aligned} \tag{8}$$

Table 1
Bearing and material parameters.

Bearing inner radius, [mm]	198.5
Bearing outer radius, [mm]	297.5
Bearing length, [mm]	200
Bearing cold radial clearance, C, [μm]	237
Bearing supply groove length, [mm]	160
Bearing supply groove width, [rad]	0.51
Supply oil temperature, [°C]	65
PTFE thickness, s, [mm]	0.5–3.0
Journal speed, Ω, [rpm]	900–2700
Oil viscosity, μ, [Pa s] at 40 °C	0.033
at 100 °C	0.0056
Oil density, [kg/m^3]	864.7
Oil specific heat, [J/KgK]	2008.5
Oil thermal conductivity, [W/(mK)]	0.13
PTFE thermal conductivity, [W/(mK)]	0.27
Steel thermal conductivity, [W/(mK)]	50
Steel to air convection, [W/(m^{2}K)]	50
Steel to oil convection, [W/(m^{2}K)]	750
PTFE thermal expansion, [K^{-1}]	1.35E-4
Steel thermal expansion, [K^{-1}]	1.11E-5
PTFE Young's modulus, E, [GPa]	0.11
PTFE Poisson's ratio, ν, [dimensionless]	0.46

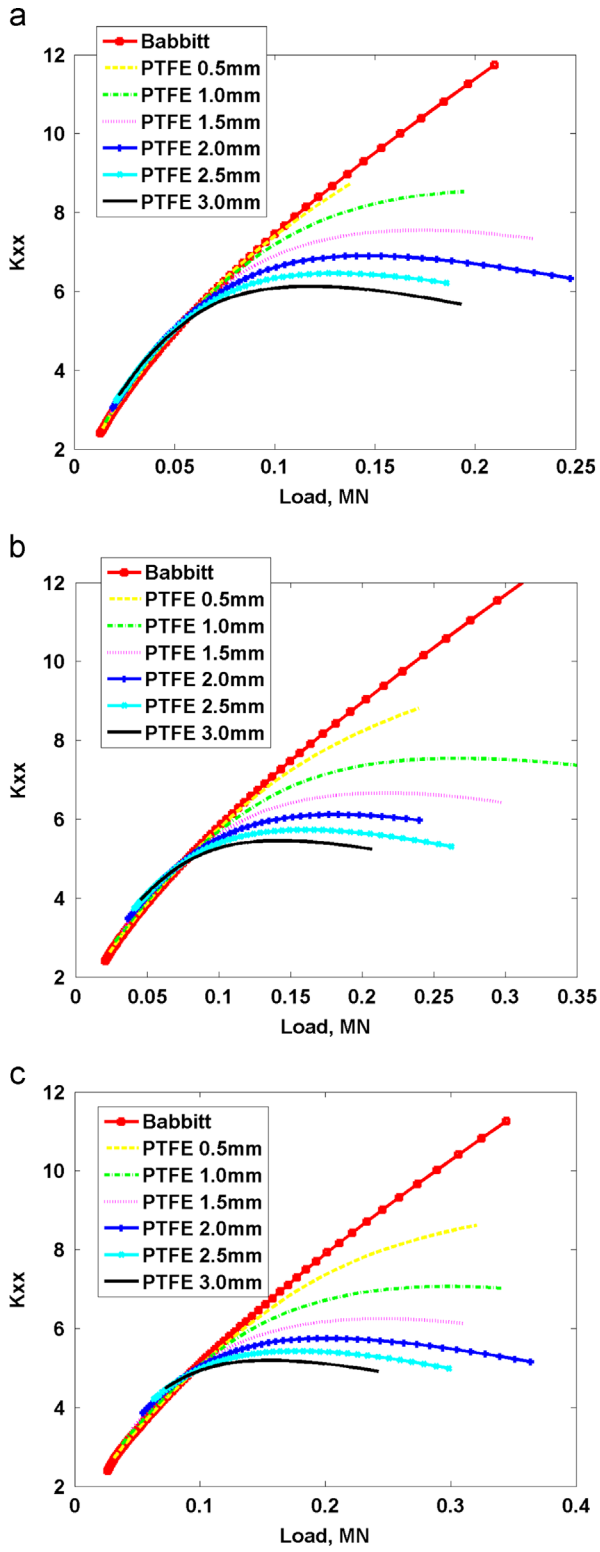

Fig. 2. Non-dimensional vertical stiffness, 900 rpm(a), 1800 rpm(b), 2700 rpm(c).

$$\frac{\partial}{\partial\theta}\left(\overline{G}\left(\overline{h}_0+F_{def}(\overline{p}_0)\right)^3\frac{\partial\overline{p}_x'}{\partial\theta}\right)+\eta\frac{\partial}{\partial\overline{z}}\left(\overline{G}\left(\overline{h}_0+F_{def}(\overline{p}_0)\right)^3\frac{\partial\overline{p}_x'}{\partial\overline{z}}\right)=\frac{\partial\left(F_{def}(\overline{p}_x')\left(1-\frac{\overline{I}}{\overline{J}}\right)\right)}{\partial\theta}$$
$$+(\cos\theta+F_{def}(\overline{p}_x))-3\frac{\partial}{\partial\theta}\left(\overline{G}\left(\overline{h}_0+F_{def}(\overline{p}_0)\right)^2F_{def}(\overline{p}_x')\frac{\partial\overline{p}_0}{\partial\theta}\right)-3\eta\frac{\partial}{\partial\overline{z}}\left(\overline{G}\left(\overline{h}_0+F_{def}(\overline{p}_0)\right)^2F_{def}(\overline{p}_x')\frac{\partial\overline{p}_0}{\partial\overline{z}}\right), \quad (9)$$

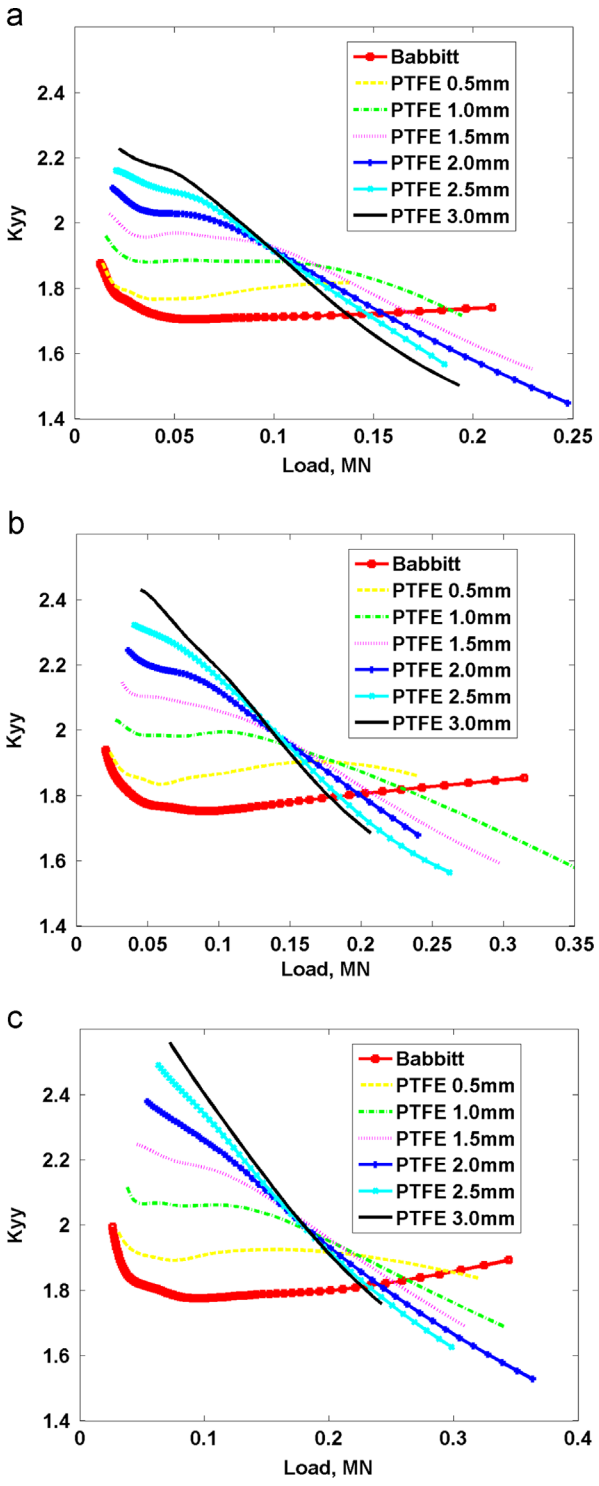

Fig. 3. Non-dimensional horizontal stiffness, 900 rpm(a), 1800 rpm(b), 2700 rpm(c).

$$\frac{\partial}{\partial\theta}\left(\overline{G}\left(\overline{h}_0+F_{def}\left(\overline{p}_0\right)\right)^3\frac{\partial\overline{p}_y'}{\partial\theta}\right)+\eta\frac{\partial}{\partial\overline{z}}\left(\overline{G}\left(\overline{h}_0+F_{def}\left(\overline{p}_0\right)\right)^3\frac{\partial\overline{p}_y'}{\partial\overline{z}}\right)=\frac{\partial\left(F_{def}\left(\overline{p}_y'\right)\left(1-\frac{\overline{I}}{\overline{J}}\right)\right)}{\partial\theta}$$
$$+\left(\sin\ \theta+F_{def}\left(\overline{p}_y\right)\right)-3\frac{\partial}{\partial\theta}\left(\overline{G}\left(\overline{h}_0+F_{def}\left(\overline{p}_0\right)\right)^2F_{def}\left(\overline{p}_y'\right)\frac{\partial\overline{p}_0}{\partial\theta}\right)-3\eta\frac{\partial}{\partial\overline{z}}\left(\overline{G}\left(\overline{h}_0+F_{def}\left(\overline{p}_0\right)\right)^2F_{def}\left(\overline{p}_y'\right)\frac{\partial\overline{p}_0}{\partial\overline{z}}\right), \tag{10}$$

Solution of (5) gives a steady-state pressure field that is based on a viscosity distribution obtained from the static analysis (see [12] for details). Further on, we assume that perturbations do not affect temperature in any manner. Under such assumption, we use viscosity derived in the process of static analysis for determining $\overline{G}$, $\overline{I}$and $\overline{J}$. Next, we use finite difference and successive-over-relaxation techniques

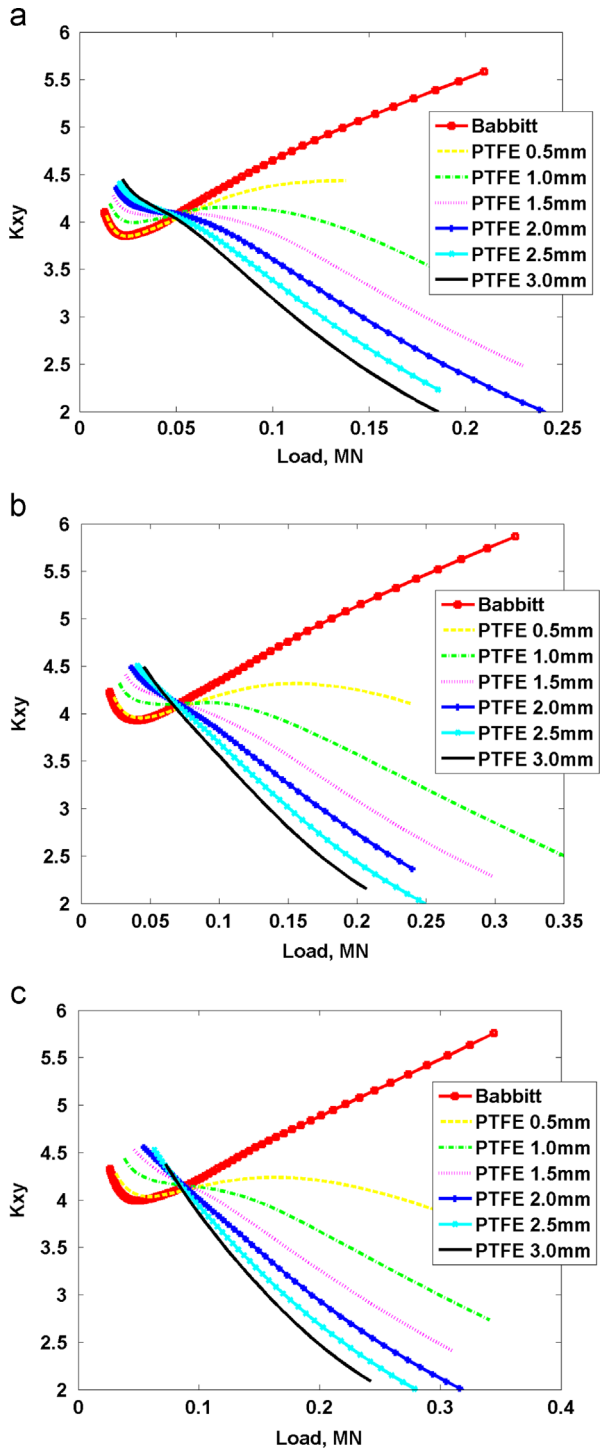

Fig. 4. Non-dimensional cross-coupled stiffness K_{xy}, 900 rpm(a), 1800 rpm(b) and 2700 rpm(c).

to solve Eqs. (6)–(10). Once the solution is obtained, we calculate stiffness and damping coefficients as follows:

$$\begin{Bmatrix} \overline{K}_{xx} \\ \overline{K}_{yx} \end{Bmatrix} = -\int_0^1 \int_0^{2\pi} \overline{p}_x \begin{Bmatrix} \cos\theta \\ \sin\theta \end{Bmatrix} d\theta dz, \tag{11}$$

$$\begin{Bmatrix} \overline{K}_{xy} \\ \overline{K}_{yy} \end{Bmatrix} = -\int_0^1 \int_0^{2\pi} \overline{p}_y \begin{Bmatrix} \cos\theta \\ \sin\theta \end{Bmatrix} d\theta dz, \tag{12}$$

$$\begin{Bmatrix} \overline{B}_{xx} \\ \overline{B}_{yx} \end{Bmatrix} = -\int_0^1 \int_0^{2\pi} \overline{p}_x' \begin{Bmatrix} \cos\theta \\ \sin\theta \end{Bmatrix} d\theta dz, \tag{13}$$

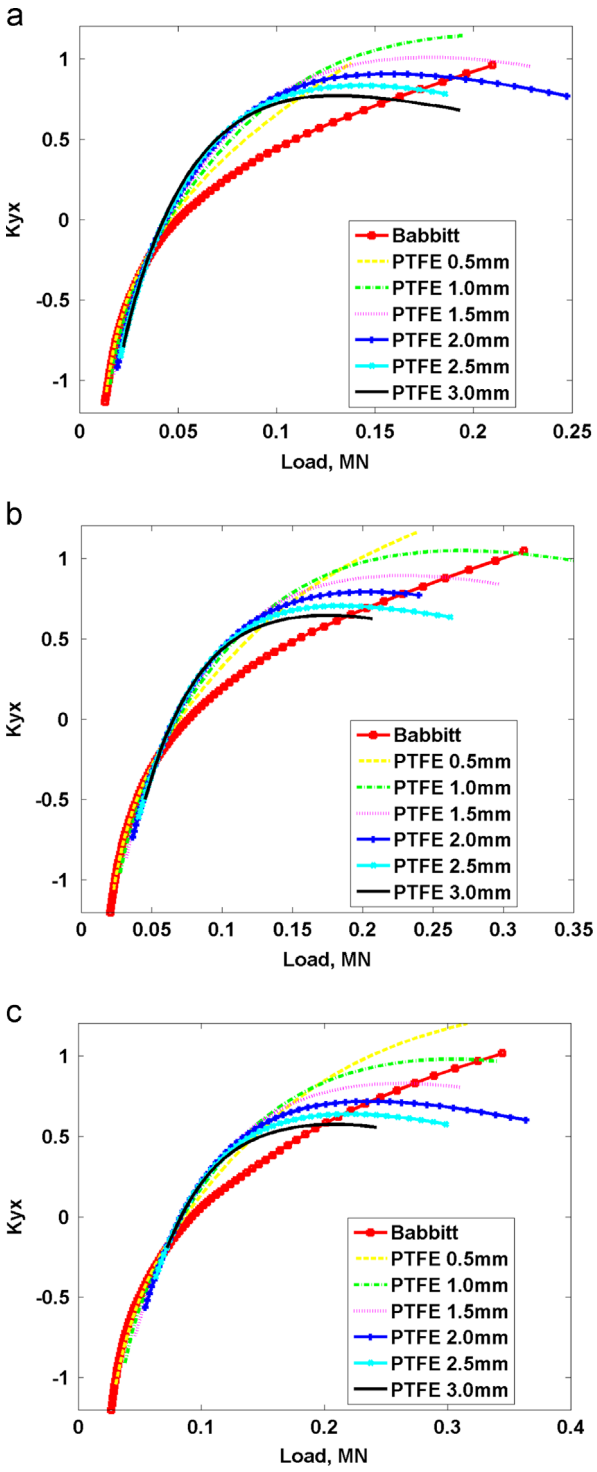

Fig. 5. Non-dimensional cross-coupled stiffness K_{yx}, 900 rpm(a), 1800 rpm(b) and 2700 rpm(c).

$$\begin{Bmatrix} \overline{B}_{xy} \\ \overline{B}_{yy} \end{Bmatrix} = -\int_0^1 \int_0^{2\pi} \overline{p}_y' \begin{Bmatrix} \cos\theta \\ \sin\theta \end{Bmatrix} d\theta dz. \tag{14}$$

By using stiffness and damping coefficients we can evaluate effective bearing stiffness

$$k_0 = \frac{K_{xx}B_{yy} + K_{yy}B_{xx} - K_{xy}B_{yx} - K_{yx}B_{xy}}{B_{xx} + B_{yy}},$$

and instability whirl frequency from

$$\left(\frac{\vartheta}{\omega}\right)^2 = \frac{(K_{xx} - k_0)(K_{yy} - k_0) - K_{xy}K_{yx}}{\omega^2 (B_{xx}B_{yy} - B_{xy}B_{yx})}.$$

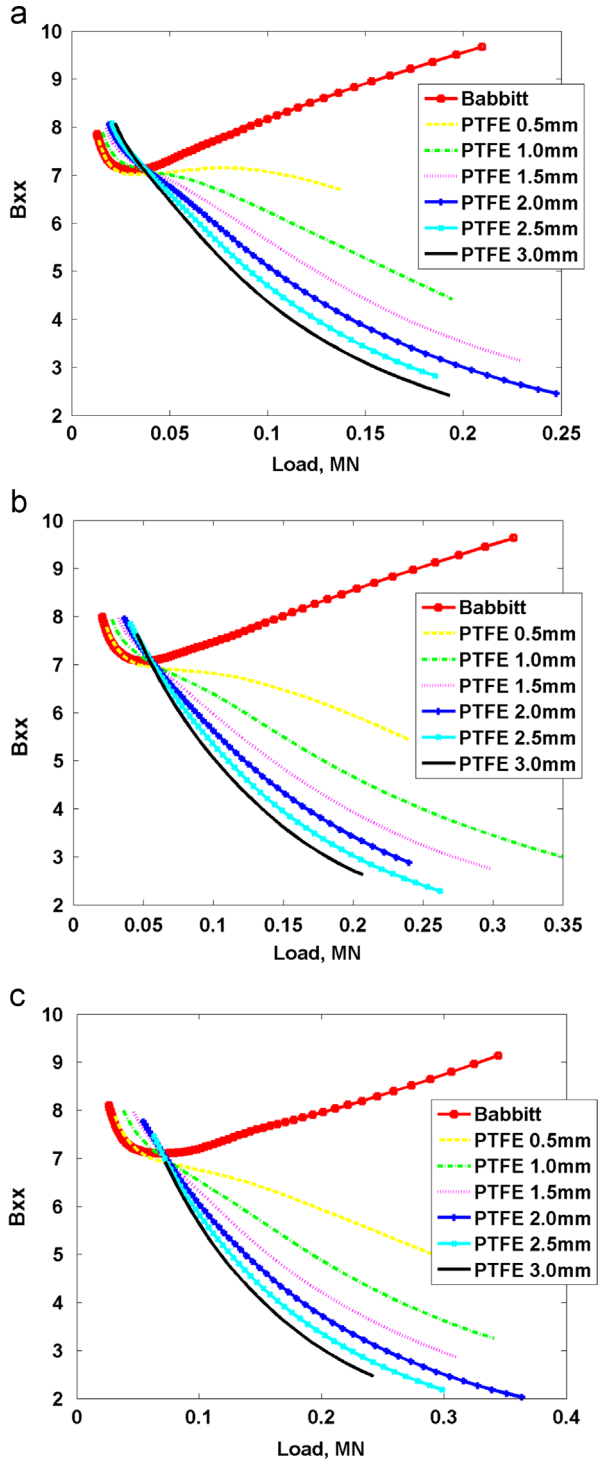

Fig. 6. Non-dimensional vertical damping, 900 rpm(a), 1800 rpm(b) and 2700 rpm(c).

Finally, critical journal mass can be evaluated as follows:

$$M_{crit} = \frac{k_0}{\vartheta^2}. \tag{15}$$

The numerical model for the iso-viscous dynamic analysis has been verified through a comparison with the Lund's model. A very good agreement was obtained as shown in [6,12]. Any further validation of the TEHD model requires experimental data for stiffness and damping that are currently unavailable.

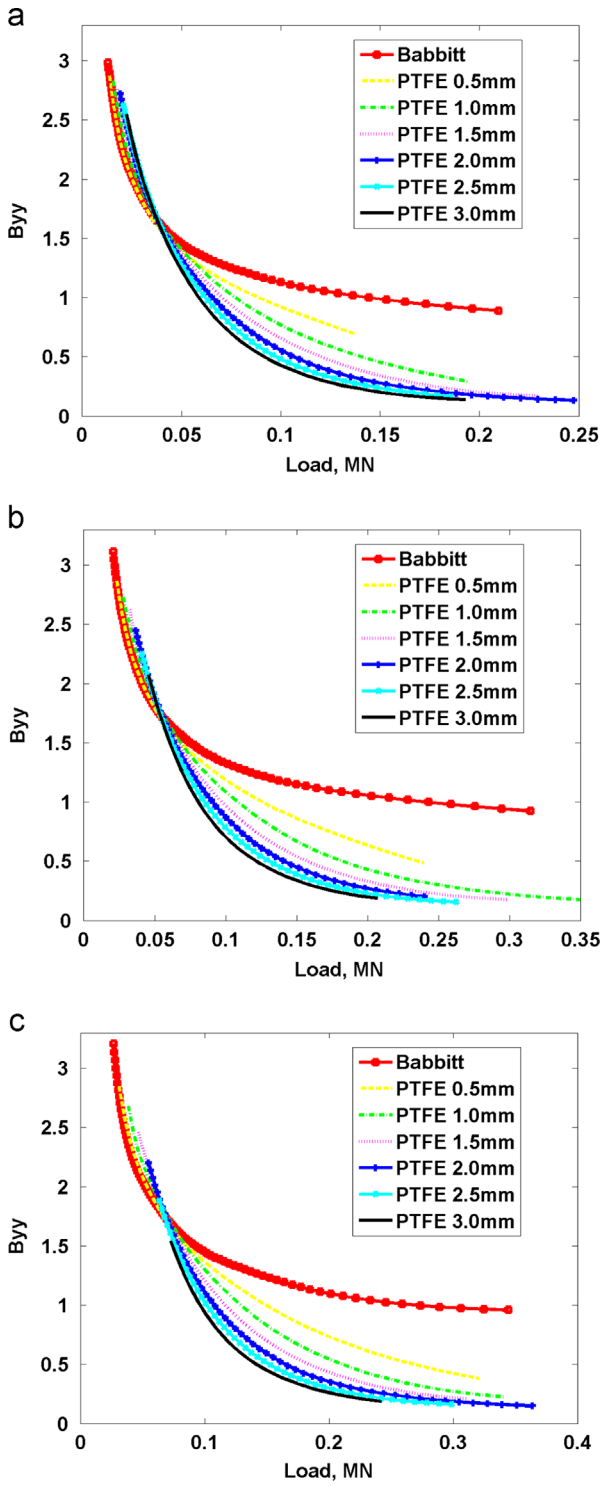

Fig. 7. Non-dimensional horizontal damping, 900 rpm(a), 1800 rpm(b) and 2700 rpm(c).

3. Results

The influence of lining compliance on bearing dynamic characteristics is evaluated by comparing a conventional babbitted bearing to a bearing with a compliant material used instead of babbitt. Properties of the compliant material are equivalent to those of PTFE (Table 1). The compliant material is assumed to be purely elastic.

Bearing and material parameters are presented in Table 1. PTFE lining thickness is varied from 0.5 to 3 mm. Journal speeds are set to 900, 1800 and 2700 rpm. The input parameters are the same as in [6], where babbitted and compliant bearings were compared in steady state operating conditions. Dynamic analysis provides stiffness and damping coefficients (as given by Eqs. (11)–(14)) and a journal critical mass, Eq. (15). For the sake of simplicity we compare non-dimensional dynamic characteristics and plot them as a function of load carrying capacity. While it is more common in the numerical studies to present data with respect to relative eccentricity we use load carrying

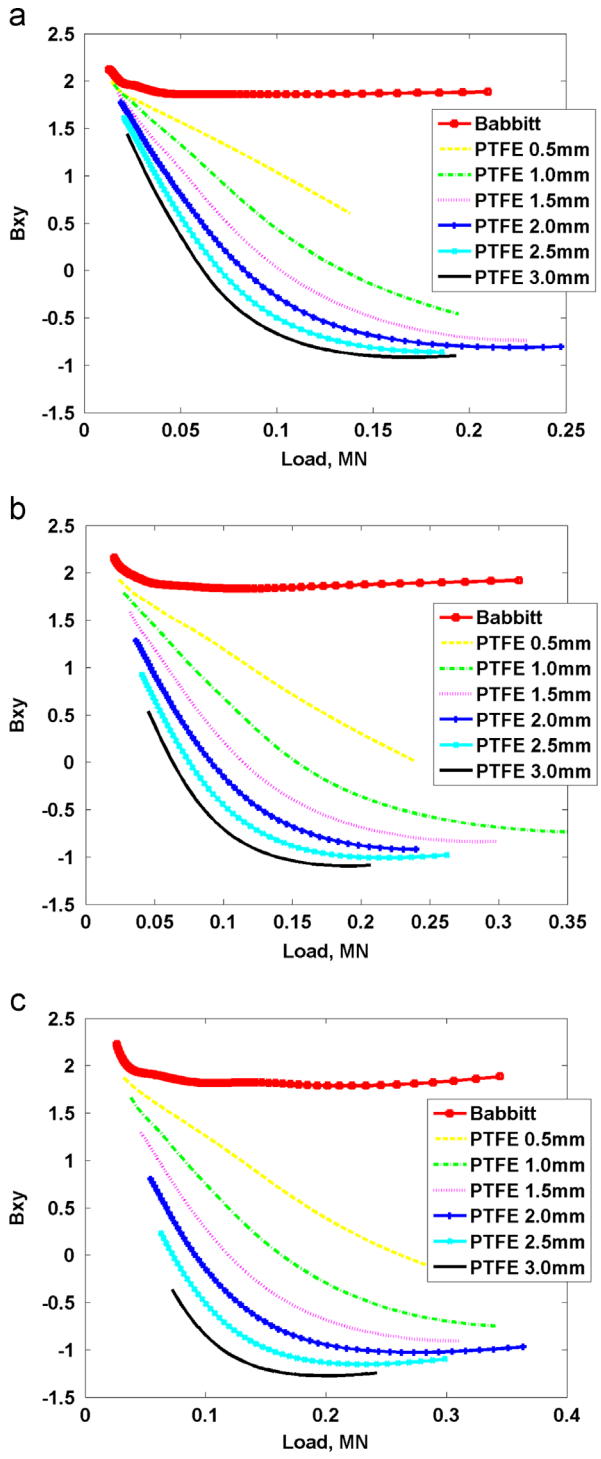

Fig. 8. Non-dimensional cross-coupled damping B_{xy}, 900 rpm(a), 1800 rpm(b) and 2700 rpm(c).

capacity. This makes it easier to evaluate what happens in the practical applications if a babbitted bearing is substituted by a compliant bearing. Furthermore, the relative eccentricity is usually evaluated based on the cold radial clearance that is measured at room/ambient temperature. During steady state operation thermal expansion of the bearing and the journal changes film thickness profile, which affects radial clearance (see [6] for details).

We start bearing comparison with non-dimensional vertical stiffness, K_{xx}, at a journal speed of 900 rpm (Fig. 2a). Nearly the same stiffness that grows with load is observed for both babbitted and compliant bearings for loads below 60 kN. At higher loads stiffness of the babbitted bearing continues to increase whilst lining deformation in the compliant bearings restrains this growth. This trend results in load intervals where stiffness of the compliant bearings is nearly constant. The effect is proportional to the lining thickness. Similar trends are observed at higher journal speeds, 1800 rpm (Fig. 2b) and 2700 rpm (Fig. 2c). In general, if compared at the same load, non-dimensional vertical stiffness decreases as a function of journal speed. An increase in speed also shifts the value of cross point load (CPL), at which K_{xx} of all bearings is the same, towards higher values.

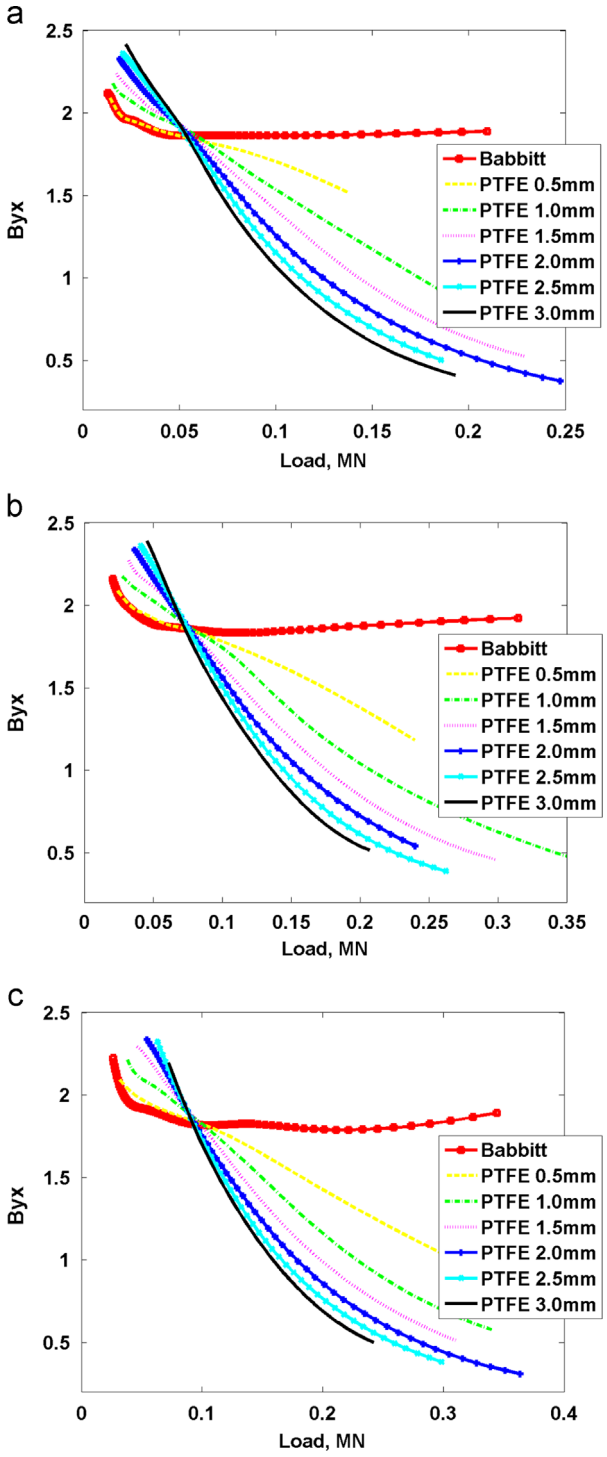

Fig. 9. Non-dimensional cross-coupled damping B_{yx}, 900 rpm(a), 1800 rpm(b) and 2700 rpm(c).

Non-dimensional horizontal stiffness, K_{yy}, is shown in Fig. 3. It is relatively constant in a wide range of loads for the babbitted bearing. Compliance of the lining increases K_{yy} at low and midrange loads while an opposite effect is observed at high loads. Here and further on by low, medium or high load we denote a load that is obtained at low, medium or high relative eccentricity. Therefore, the same load value can be considered as large or medium depending on the journal speed (e.g. a load of 0.2 MN at 900 and 2700 rpm). CPL value, at which stiffness of babbited and compliant bearings is the same, depends on the lining thickness. For example, at 900 rpm it is 0.15 MN if the 2.5 mm compliant lining bearing is selected or nearly 0.2 MN if lining thickness is reduced to 1 mm, Fig. 3a. The CPL becomes lower if the compliant lining thickness increases or journal speed decreases. Another group of CPLs can be observed if only compliant bearings are compared. These CPL values follow the same trend: higher values correspond to higher speeds and thinner linings.

Non-dimensional cross-coupled stiffness, K_{xy}, is shown in Fig. 4. It increases with load for the babbitted bearings and decreases for the compliant bearings. At 900 rpm, compliant bearings provide higher K_{xy} for loads below approximately 50 kN and lower K_{xy} otherwise,

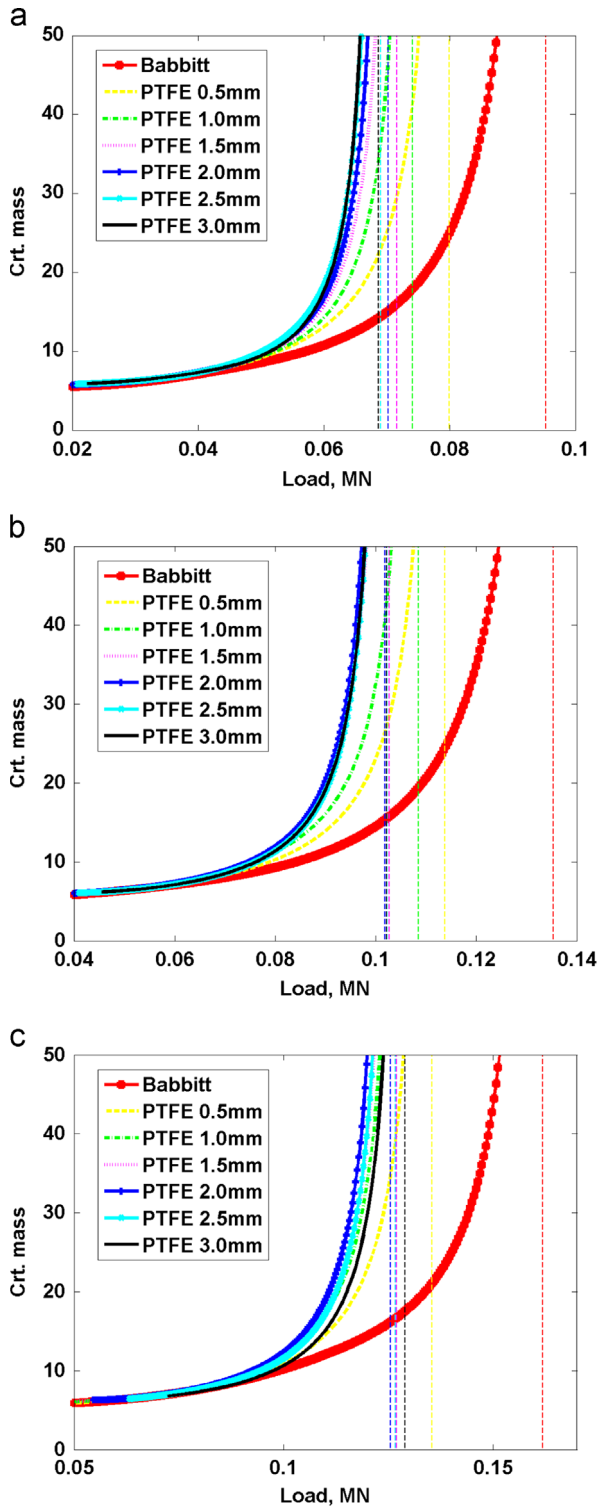

Fig. 10. Non-dimensional critical journal mass, 900 rpm(a), 1800 rpm(b) and 2700 rpm(c).

Fig. 4a. The interval of CPL values is very narrow, from approximately 48 to 60 kN. As the journal speed increases the CPL interval remains narrow but CPL values significantly increase. K_{xy} in the babbitted bearing decreases with speed at medium and high loads. In the same load interval K_{xy} in the compliant bearing increases with speed.

Non-dimensional cross-coupled stiffness, K_{yx}, is shown in Fig. 5. Compliance reduces value of K_{yx} at low and high loads and increases it at medium loads, producing a bow-like shape of the trend. For example, a 3 mm compliant lining bearing at 900 rpm, if compared to the babbitted bearing, provides lower K_{yx} at loads below 30 kN or above 160 kN but higher K_{yx} in the interval from 30 kN to 160 kN, Fig. 5a. At low loads K_{yx} is negative for all bearings. Increasing speed decreases K_{yx} and even makes stiffness negative at low loads. CPL values increase with the journal speed.

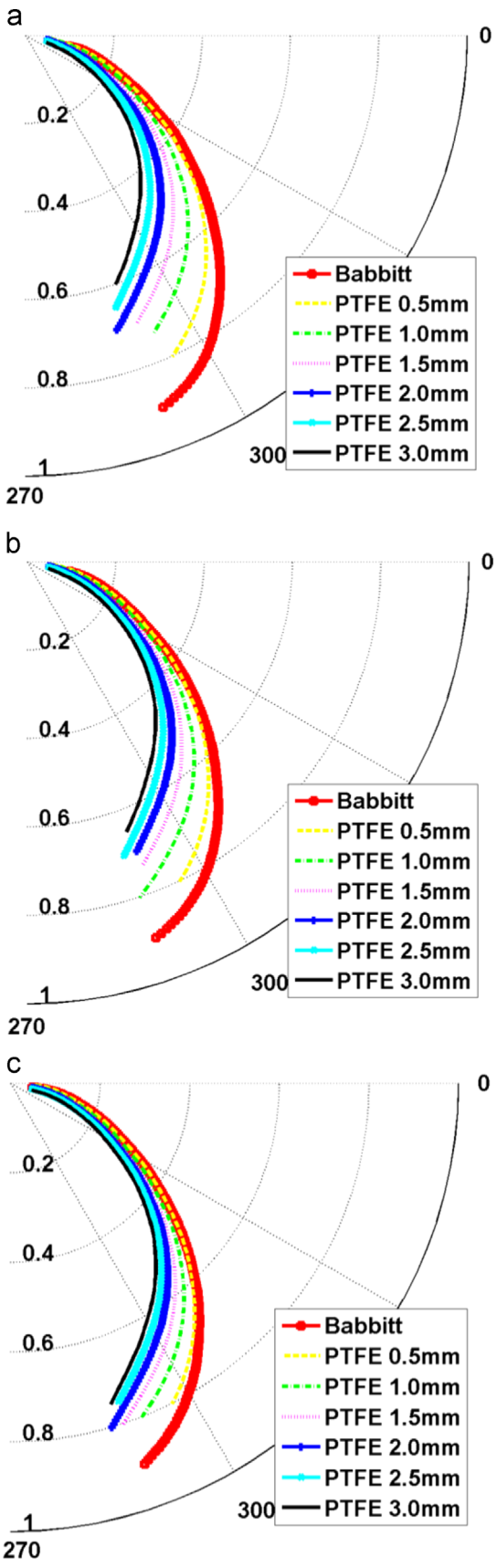

Fig. 11. Journal centre equilibrium position (locus), 900 rpm(a), 1800 rpm(b) and 2700 rpm(c).

Table 2
Test configurations.

Effect	Configuration w/o Effect	Configuration with Effect
PTFE thermal expansion	Babbitt	PTFE w/o def
PTFE mechanical deformation	Babbitt	PTFE w/o exp
Increased cold clearance	Babbitt	Babbitt Cr
PTFE thermal expansion	PTFE w/o exp	PTFE 2.0 mm
PTFE mechanical deformation	PTFE w/o def	PTFE 2.0 mm
Increased cold clearance	PTFE 2.0 mm	PTFE 2.0 mm Cr

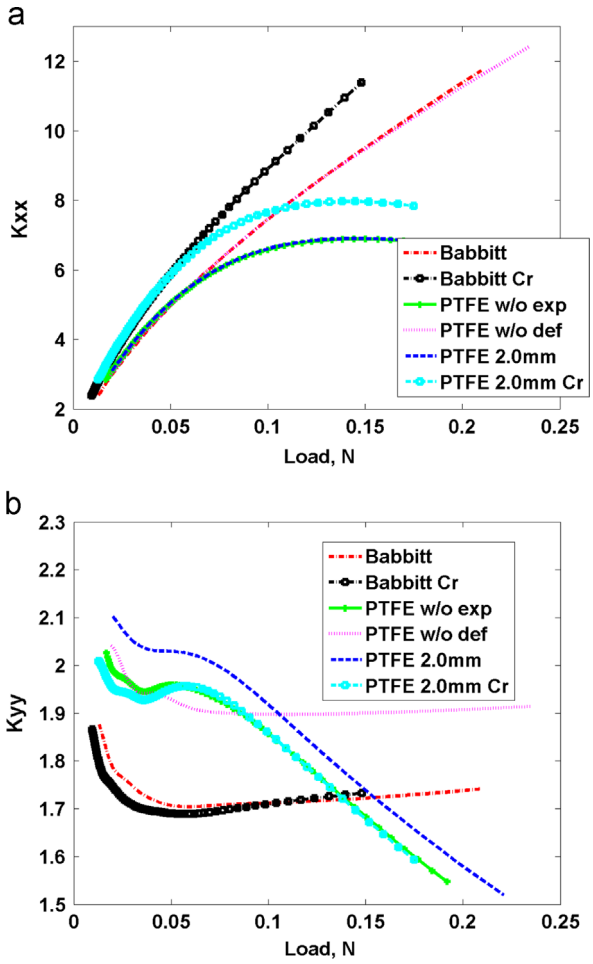

Fig. 12. Non-dimensional vertical (a) and horizontal (b) stiffness, 900 rpm.

Non-dimensional vertical damping B_{xx} shows trends similar to K_{xy} as depicted in Fig. 6. At 900 rpm the CPL values are in the vicinity of 37 kN, Fig. 6a. They then increase to 55 kN at 1800 rpm and 73 kN at 2700 rpm. B_{xx} increases with compliance if load is lower than the CPL value but decreases otherwise.

Fig. 7 shows a strong decrease in non-dimensional horizontal damping, B_{yy}, as a function of load for all bearings. At low loads compliance provides a slight increase in B_{yy} compared to the babbitted bearing and lower B_{yy} otherwise. CPL value is 38.5 kN at 900 rpm, 56 kN at 1800 rpm and 69.5 kN at 2700 rpm.

Non-dimensional cross-coupled damping, B_{xy}, is marginally affected by speed or load in case of the babbitted bearing as shown in Fig. 8. Compliance decreases B_{xy} at all loads and speeds. The magnitude of the decrease initially grows with load but then levels off. Compliance also results in the onset of negative damping. The load, at which B_{xy} changes its sign, decreases if the compliant lining becomes thicker or journal speed is reduced.

Non-dimensional cross-coupled damping, B_{yx}, is shown in Fig. 9. While it is well known that B_{xy} and B_{yx} are identical in the case of babbitted bearings [9], compliant lining bearings do not exhibit this property if perturbation of the lining deformation is taken into account as shown in [10–12,14,15]. The difference in behaviour of B_{xy} and B_{yx} (compare Figs. 8 and 9) is therefore observed in our case. At 900 rpm compliance increases B_{yx} at loads below 55 kN. The CPL interval at 1800 rpm is 65–81 kN. A further shift to 84–100 kN is observed at 2700 rpm. Compliance does not result in negative B_{yx} damping.

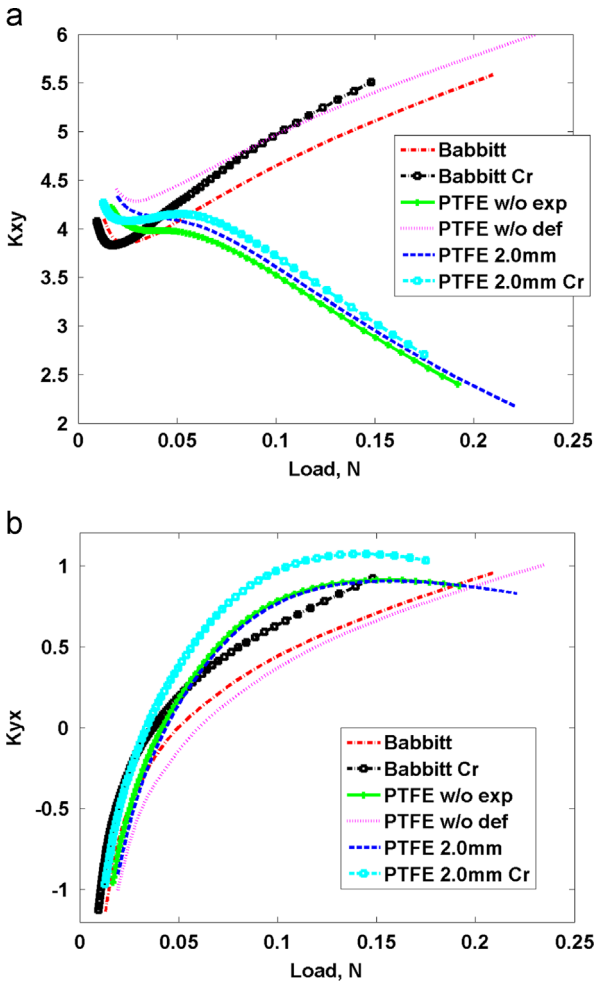

Fig. 13. Non-dimensional cross-coupled stiffness, 900 rpm.

Fig. 10 shows variation in non-dimensional critical journal mass as a function of load. The area above each line corresponds to instability region. A higher value of M_{crit} means an improvement in bearing stability characteristics. At all journal speeds considered, an increase in lining thickness and thus compliance results in smaller instability region.

A further insight into compliant bearing dynamic behaviour can be gained by analysing journal centre loci. Fig. 11 shows equilibrium positions of journal centre for the babbitted and compliant bearings. At the same load lining compliance reduces journal eccentricity and attitude angle. This effect becomes more pronounced with increasing loads and speeds.

4. Discussion

The influence of mechanical and thermal deformations on bearing dynamic characteristics is clarified using a number of special test configurations in a similar manner as shown in [6] for the steady state operating parameters. The test configurations used in the analysis are summarised in Table 2. First, two configurations from the Results section: the babbitted bearing (Babbitt), configuration 1, and the compliant bearing with a 2 mm PTFE lining (PTFE 2.0 mm), configuration 2, are selected. Next, a compliant bearing with a 2 mm PTFE lining without its mechanical deformation (PTFE w/o def) is compared to configuration 2. This will explain how compliance affects bearing dynamics. A comparison of the case (PTFE w/o def) with configuration 1 will show the effect of PTFE thermal expansion.

Since thermal expansions of the shaft, bearing and especially PTFE lining reduce the radial clearance two additional configurations are considered: babbitted and 2 mm PTFE lining bearings with cold clearances increased by 43 μm (Babbitt Cr and PTFE 2.0 mm Cr). The last configuration considered: 2 mm PTFE lining bearing without thermal deformation of the lining (PTFE w/o exp) but with thermal expansion of the shaft and steel housing as well as mechanical deformation of the lining. A comparison of this configuration with configuration 2 will show the effect of thermal expansion of the compliant layer on stiffness, damping and M_{crit}. A further comparison of this configuration with configuration 1 will indicate how PTFE lining compliance and thermal insulation affect bearing dynamic characteristics. We only show results for 900 rpm journal speed to keep the number of figures and length of the paper within allowable limits.

Non-dimensional vertical stiffness, K_{xx}, is shown in Fig. 12a. There is no visible effect of lining thermal expansion on K_{xx}. Mechanical deformation decreases vertical stiffness at medium and high loads, i.e. when the deformation of the lining is high enough. An increase in cold radial clearance provides higher K_{xx}.

Fig. 12b shows non-dimensional horizontal stiffness, K_{yy}. Thermal expansion increases K_{yy} in the entire load range. Influence of mechanical deformation is more complex and depends on operating conditions. Mechanical deformation increases K_{yy} at low loads but

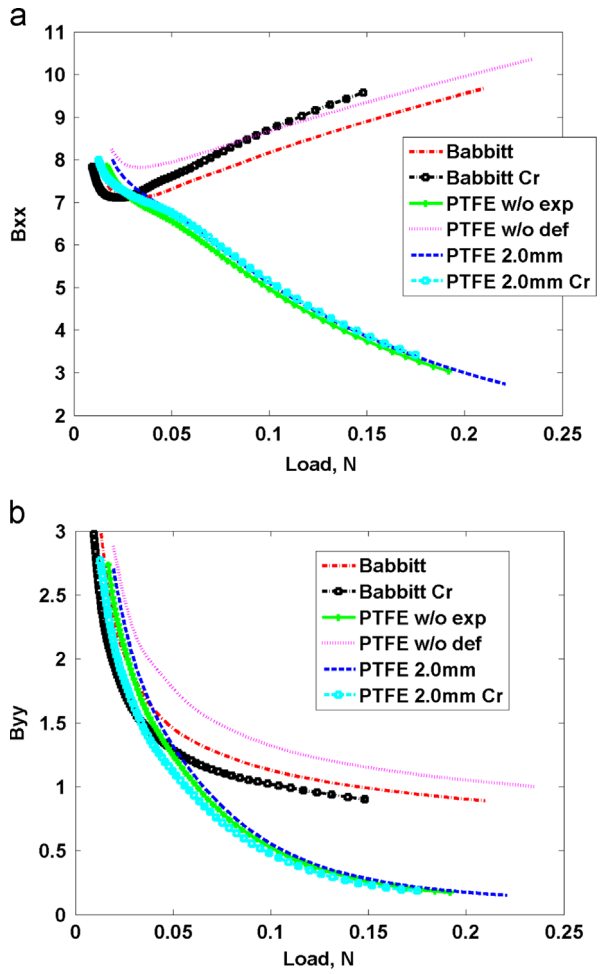

Fig. 14. Non-dimensional vertical (a) and horizontal (b) damping, 900 rpm.

decreases it at high loads. Larger radial clearance has a slight decreasing effect in the babbitted bearing at low loads but provides a stronger reduction in K_{yy} in the 2 mm PTFE lining bearing.

Non-dimensional cross-coupled stiffness, K_{xy}, is shown in Fig. 13a. Thermal expansion slightly increases stiffness in the entire load range. Mechanical deformation decreases K_{xy}. The largest reduction occurs at the highest load. Larger radial clearance slightly increases bearing stiffness except at the lightest loads. The clearance effect is more pronounced for the babbitted bearing.

Fig. 13b shows non-dimensional cross-coupled stiffness, K_{yx}. Thermal expansion has almost no effect on K_{yx} while mechanical deformation increases it except at the highest load. Large radial clearance increases K_{yx} in babbitted and compliant bearings

Non-dimensional vertical damping, B_{xx}, is shown in Fig. 14a. Mechanical deformation of the compliant lining significantly decreases B_{xx}. Lining thermal expansion has only a slight effect on B_{xx}. Radial clearance has almost no impact on B_{xx} in compliant bearings while it increases B_{xx} with load in the babbitted bearing.

Similar effect of compliance can be seen for non-dimensional horizontal damping, B_{yy}. Mechanical deformation significantly decreases it while thermal expansion slightly increases it as shown in Fig. 14b. Large radial clearance, on the contrary, decreases horizontal damping.

Non-dimensional cross-coupled damping coefficients B_{xy} and B_{yx} are almost unaffected by the thermal expansion as shown in Fig. 15. Radial clearance has almost no effect on B_{xy} and slightly increases B_{yx}. Mechanical deformation decreases cross-coupled damping in both cases with a stronger effect on B_{xy}.

Fig. 16 shows non-dimensional critical journal mass as a function of load. Both radial clearance and mechanical deformation improve stability by increasing critical journal mass. Thermal expansion has a slight but an opposite effect on M_{crit}.

5. Conclusions

The effect of compliance on journal bearing dynamic characteristics has been investigated. A numerical three-dimensional THD model including lining deformation has been developed for the analysis. Bearings with different compliant lining thicknesses are compared to a conventional babbitted bearing in terms of stiffness and damping coefficients, critical journal mass and loci. It is shown that compliant lining provides:

- a decrease in vertical stiffness;
- an increase in horizontal stiffness at low loads and a decrease at high loads;
- an increase in vertical and horizontal damping at small loads and a decrease at high loads;

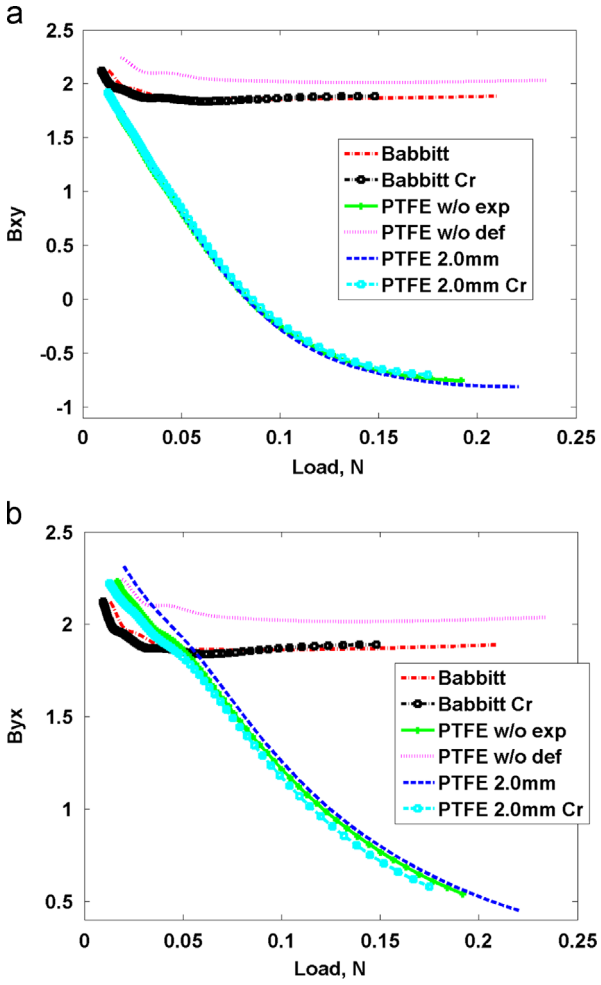

Fig. 15. Non-dimensional cross-coupled damping, 900 rpm.

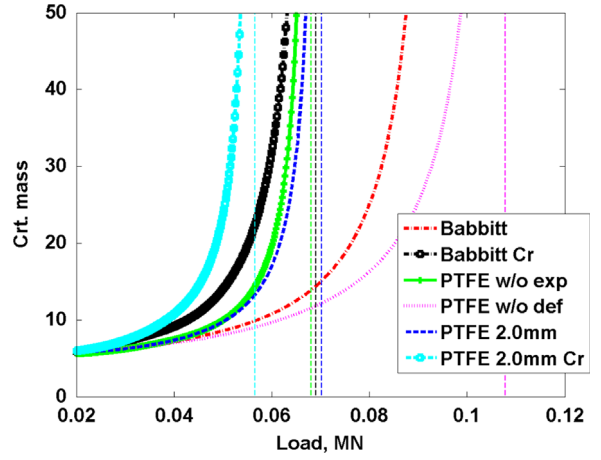

Fig. 16. Non-dimensional critical journal mass, 900 rpm.

- an improved bearing stability;
- a lower eccentricity and attitude angle.

An in-depth investigation on the contribution of mechanical and thermal deformations to bearing dynamic characteristics shows that thermal expansion increases horizontal K_{yy} and cross-coupled K_{xy} stiffness, slightly reduces journal critical mass and therefore has a negative influence on bearing stability. On the other hand, mechanical deformation is found to decrease damping, reduce vertical and cross-coupled K_{xy} stiffness. It also increases horizontal stiffness at low loads, cross-coupled K_{yx} stiffness in almost entire load range and significantly increases bearing stability. Finally, an increase in radial clearance increases non-dimensional vertical and cross-coupled stiffness, decreases horizontal damping and improves stability.

Acknowledgements

The financial support provided by the Swedish Energy Agency, ABB Automation Technologies, and Siemens Industrial Turbomachinery is gratefully acknowledged.

References

[1] Simmons GF, Glavatskih S, Müller M, Byheden Å, Prakash B. Extending performance limits of turbine oils. Tribol Int 2014;69:52–60.
[2] Markin D, McCarthy D, Glavatskih S. A FEM approach to simulation of tilting pad thrust bearing assemblies. Tribol Int 2003;36:807–14.
[3] Glavatskih S. Evaluating thermal performance of a PTFE-faced tilting pad thrust bearing. J Tribol 2003;125(2):319–24.
[4] Glavatskih SB, Fillon M. TEHD analysis of thrust bearings with PTFE-faced pads. J Tribol 2006;128(1):49–58.
[5] Golchin A, Simmons GF, Glavatskih SB. Break-away friction of PTFE materials in lubricated conditions. Tribol Int 2012;48:54–62.
[6] Kuznetsov E, Glavatskih S, Fillon M. THD analysis of compliant journal bearing considering liner deformation. Tribol Int 2011;44(12):1629–41.
[7] Heshmat CA, Heshmat H. Analysis of gas-lubricated, multileaf foil journal bearings with backing springs. J Tribol 1995;117(3):437–43.
[8] San Andrés L, Kim TH. Analysis of gas foil bearings integrating FE top foil models. Tribol Intl 2009;42(1):111–20.
[9] Lund JW, Thomsen KK. A calculation method and data for the dynamic coefficients of oil-lubricated journal bearings. Top Fluid Bear Rotor Bear Syst 1978:1–28.
[10] Zhang Z, Mao Q, Xu H. The effect of dynamic deformation on dynamic properties and stability of cylindrical journal bearings. Tribol Ser 1987;11:262–6.
[11] Lahmar M, Haddad A, Nicolas D. Elastohydrodynamic analysis of one-layered journal bearings. Proc Inst Mech Eng J 1998;212:193–205.
[12] Kuznetsov E, and Glavatskih S. Dynamic characteristics of a 2 axial groove journal bearing with a PTFE lining, In: Proc. 16th Int. Col. Trib. Auto. and Ind. Lub, 2008,.
[13] Rao TVVLN, Biswas S, Hirani H, Athre K. An analytical approach to evaluate dynamic coefficients and nonlinear transient analysis of a hydrodynamic journal bearing. Tribol Trans 2000;43:109–15.
[14] Attia Hili M, Bouaziz S, Maatar M, Fakhfakh T, Haddar M. Hydrodynamic and elastohydrodynamic studies of a cylindrical journal bearing. J Hydrodyn 2010;22:155–63.
[15] Lahmar M, Ellagoune S, Bou-Said B. Elastohydrodynamic lubrication analysis of a compliant journal bearing considering static and dynamic deformations of the bearing lining. Tribol Trans 2010;53:349–68.
[16] Durany J, Pereira J, Varas F. Dynamical stability of journal-bearing devices through numerical simulation of thermohydrodynamic models. Tribol Int 2010;43:1703–18.
[17] Tanaka M, Hatakenaka K. Thermohydrodynamic lubrication model of journal bearings. Jpn J Tribol 2004;49:467–77.
[18] Cha M, Kuznetsov E, Glavatskih S. A comparative linear and nonlinear dynamic analysis of compliant cylindrical journal bearings. Mech Mach Theory 2013;64:80–92.